Contribution from the Department of Chemistry, Harvard University, Cambridge, Massachusetts 02138, and the Francis Bitter National Magnet Laboratory, Massachusetts Institute of Technology, Cambridge, Massachusetts 02139

# Electronic Properties of Single- and Double-$MoFe_3S_4$ Cubane-Type Clusters

P. K. MASCHARAK,[1a] G. C. PAPAEFTHYMIOU,[1b] W. H. ARMSTRONG,[1a] S. FONER,[1b] R. B. FRANKEL,[1b] and R. H. HOLM*[1a]

*Received December 28, 1982*

Electronic properties of the single-cubane clusters $[MoFe_3S_4(SR)_3(3,6\text{-}R'_2cat)(solv)]^{2-,3-}$ and $[MoFe_3S_4(SR)_4(3,6\text{-}R'_2cat)]^{3-}$ and the double-cubane cluster $[Mo_2Fe_6S_8(SR)_6(3,6\text{-}R'_2cat)_2]^{4-}$ (3,6-$R'_2$cat = 3,6-diallyl- or 3,6-di-*n*-propylcatecholate, solv = solvent) have been investigated by Mössbauer and EPR spectroscopy and magnetization measurements. In most cases R = *p*-$C_6H_4Cl$ and R′ = allyl. It is shown that oxidized ($[MoFe_3S_4]^{3+}$) single cubanes consist of electronically delocalized, antiparallel spin-coupled clusters with $S = {}^3/_2$ ground states. Properties of one reduced ($[MoFe_3S_4]^{2+}$) single cubane are similar, and its ambient-temperature magnetic moment indicates a $S = 2$ ground state. The isomer shift difference between the oxidized and reduced clusters reveals that the $Fe_3$ portions are those primarily affected by electron gain or loss. The bridged double cubane, containing two $[MoFe_3S_4]^{3+}$ subclusters linked by two Mo–(SR)–Fe bridges, exhibits subcluster spin coupling resulting in a singlet ground state. Low-temperature magnetization data for the triply bridged double cubane $[Mo_2Fe_6S_8(SR)_9]^{3-}$ reveals much weaker subcluster interaction and a quartet ground state for each subcluster. Isomer shifts, quadrupole splittings, and hyperfine coupling constants are presented as well as a typical single-cubane EPR spectrum. Current interpretations of the Mössbauer, NMR, and EPR spectral properties of $MoFe_3S_4$ clusters are summarized. Comparison of certain electronic properties with those of the native $S = {}^3/_2$ Mo–Fe–S cluster of nitrogenase reveals a number of similarities. This information, together with EXAFS and X-ray structural data, demonstrates that some electronic and geometrical features of $MoFe_3S_4$ clusters approach those of the native cluster. These results encourage further synthetic attempts directed toward attainment of Mo–Fe–S clusters whose Fe:Mo atom ratios are closer to that ((6–8):1) of the native cluster.

## Introduction

In the rapidly expanding area of heteronuclear $MFe_3S_4$ cubane-type clusters (M = Mo, W) two general structural categories, comprised of species having two variously bridged subclusters or a single cluster, have emerged. Double cubanes include triply bridged $[M_2Fe_6S_8(\mu\text{-}S)(\mu\text{-}SR)_2(SR)_6]^{3-}$,[2-4] $[M_2Fe_6S_8(\mu\text{-}SR)_3(SR)_6]^{3-}$ (**1**),[2-6] and $[M_2Fe_7S_8(\mu\text{-}SR)_6(SR)_6]^{3-,4-}$[3,7] and doubly bridged $[M_2Fe_6S_8(\mu\text{-}SR)_2(SR)_4(3,6\text{-}R'_2cat)_2]^{4-}$ (**4**; R′ = allyl, *n*-Pr, cat = catecholate).[8-10] Single cubanes are of two types, the solvated clusters $[MFe_3S_4(SR)_3(3,6\text{-}R'_2cat)(solv)]^{2-}$ (**5**)[8-10] and the ligated clusters $[MFe_3S_4(SR)_3(3,6\text{-}R'_2cat)L]^{2-,3-}$ (**6**).[8,10-13] Reactions 1–3, which afford **5**–**7** from the precursor double cubane **4**, are shown in Figure 1 together with schematic structural formulas for clusters **1**–**7**.

In addition to clusters produced directly by synthesis, one-electron redox products that retain the structural elements of the oxidized forms can be obtained by chemical or electrochemical means. Thus the triply bridged trianion **1** can be reduced to **2** and **3** in chemically reversible one-electron steps, forming the electron-transfer series 4.[3,14,15] An example of the terminal reduced member **3** has been isolated and structurally characterized.[14] In this series electrons are added successively to individual subclusters,[14] resulting in reduction of the initial core oxidation level $\alpha = [MoFe_3S_4]^{3+}$ to $\beta = [MoFe_3S_4]^{2+}$. Consistent with this behavior is the reversible one-electron reduction of the solvated single cubanes **5** to **7**[12,16] (reaction 5) in the same potential interval (ca. −1.0 to −1.5 V vs. SCE) as that for the traversal of series 4.

The clusters **1** and their methoxide-bridge variants $[M_2Fe_6S_8(\mu\text{-}OMe)_3(SR)_6]^{3-}$, being among the first $MFe_3S_4$-type species synthesized,[2,6] have been the objects of detailed electronic structural studies. Extensive Mössbauer,[2,14,15] NMR,[3,6] and EPR[17] spectral and magnetic susceptibility[14,17] data have been collected and analyzed. Important electronic structural properties addressed in these investigations include ground spin states, spin coupling within and between bridged subclusters, metal site charge (oxidation state) distributions, electron delocalization between $\alpha$ and $\beta$ oxidation levels, and dominant isotropic interactions in NMR spectra. In the present work the Mössbauer, EPR, and magnetization properties of the more recently synthesized clusters **4**, **6**, and **7** (M = Mo) have been investigated in order to clarify certain of the preceding properties. Because of the different bridge structures in **4** vs. **1** and the absence of an appended, potentially perturbing second cluster in the single cubanes **6** and **7**, significant differences in certain electronic properties are anticipated and have been found. This investigation forms part of our continuing development of $MoFe_3S_4$ clusters as initial structural and electronic models of the FeMo cofactor (FeMo-co) of nitrogenase. Our approach to a synthetic representation of FeMo-co and many of the results obtained thus far have been reviewed elsewhere.[18,19]

## Experimental Section

**Preparation of Compounds.** The following compounds were obtained by published methods: $(Et_4N)_3[Mo_2Fe_6S_8(S\text{-}p\text{-}C_6H_4Cl)_9]$ (**1**);[6] $(Et_4N)_4[Mo_2Fe_6S_8(SEt)_6(Pr_2cat)_2]$,[9] $(Et_4N)_4[Mo_2Fe_6S_8(S\text{-}p\text{-}C_6H_4Cl)_6((al)_2cat)_2]$ (**4**);[9] $(Et_4N)_3[MFe_3S_4(S\text{-}p\text{-}C_6H_4Cl)_3((al)_2cat)L]$

(1) (a) Harvard University. (b) MIT.
(2) Wolff, T. E.; Berg, J. M.; Hodgson, K. O.; Frankel, R. B.; Holm, R. H. *J. Am. Chem. Soc.* **1979**, *101*, 4140.
(3) Wolff, T. E.; Power, P. P.; Frankel, R. B.; Holm, R. H. *J. Am. Chem. Soc.* **1980**, *102*, 4694.
(4) Palermo, R. E.; Power, P. P.; Holm, R. H. *Inorg. Chem.* **1982**, *21*, 173.
(5) Christou, G.; Garner, C. D.; Mabbs, F. E.; King, T. J. *J. Chem. Soc., Chem. Commun.* **1978**, 740. Acott, S. R.; Christou, G.; Garner, C. D.; King, T. J.; Mabbs, F. E.; Miller, R. M. *Inorg. Chim. Acta* **1979**, *35*, L337. Christou, G.; Garner, C. D.; Miller, R. M.; King, T. J. *J. Inorg. Biochem.* **1979**, *11*, 349.
(6) Christou, G.; Garner, C. D. *J. Chem. Soc., Dalton Trans.* **1980**, 2354.
(7) Wolff, T. E.; Berg, J. M.; Power, P. P.; Hodgson, K. O.; Holm, R. H. *Inorg. Chem.* **1980**, *19*, 430.
(8) Armstrong, W. H.; Holm, R. H. *J. Am. Chem. Soc.* **1981**, *103*, 6246.
(9) Armstrong, W. H.; Mascharak, P. K.; Holm, R. H. *J. Am. Chem. Soc.* **1982**, *104*, 4373.
(10) Mascharak, P. K.; Smith, M. C.; Armstrong, W. H.; Burgess, B. K.; Holm, R. H. *Proc. Natl. Acad. Sci. U.S.A.* **1982**, *79*, 7056.
(11) Armstrong, W. H.; Mascharak, P. K.; Holm, R. H. *Inorg. Chem.* **1982**, *21*, 1699.
(12) Mascharak, P. K.; Armstrong, W. H. Mizobe, Y.; Holm, R. H. *J. Am. Chem. Soc.* **1983**, *105*, 475.
(13) Palermo, R. E.; Holm, R. H. *J. Am. Chem. Soc.* **1983**, *105*, 4310.
(14) Christou, G.; Mascharak, P. K.; Armstrong, W. H.; Papaefthymiou, G. C.; Frankel, R. B.; Holm, R. H. *J. Am. Chem. Soc.* **1982**, *104*, 2820.
(15) Christou, G.; Garner, C. D.; Miller, R. M.; Johnson, C. E.; Rush, J. D. *J. Chem. Soc., Dalton Trans.* **1980**, 2363.
(16) Mizobe, Y.; Mascharak, P. K.; Palermo, R. E.; Holm, R. H. *Inorg. Chim. Acta*, in press.
(17) Christou, G.; Collison, D.; Garner, C. D.; Acott, S. R.; Mabbs, F. E.; Petrouleas, V. *J. Chem. Soc., Dalton Trans.* **1982**, 1575.
(18) Holm, R. H. *Chem. Soc. Rev.* **1981**, *10*, 455.
(19) Holm, R. H.; Armstrong, W. H.; Christou, G.; Mascharak, P. K.; Mizobe, Y.; Palermo, R. E.; Yamamura, T. In "Biomimetic Chemistry"; Yoshida, Z., Ise, N., Eds.; Elsevier: New York, 1983; pp 79–99.

0020-1669/83/1322-2851$01.50/0 

Table I. Magnetic and Mössbauer Spectral Data for Mo–Fe–S Clusters

| compd | $\mu_{eff}$,[a] $\mu_B$ | $T$, K | $\delta$,[b] mm/s | $\Delta E_Q$,[c] mm/s | $\Gamma$,[d] mm/s | % $A$[e] |
|---|---|---|---|---|---|---|
| $(Et_4N)_3[MoFe_3S_4(S\text{-}p\text{-}C_6H_4Cl)_4((al)_2cat)]$ (6) | | 120 | 0.30 | 1.18 | 0.46 | 64 |
| | | | 0.30 | 1.60 | 0.52 | 36 |
| solid | 4.08 | 80 | 0.31 | 1.14 | 0.46 | 66 |
| | | | 0.28 | 1.76 | 0.46 | 34 |
| MeCN soln | 4.03 | 130 | 0.31 | 0.81 | 0.40 | 49 |
| | | | 0.31 | 1.24 | 0.40 | 51 |
| | | 80 | 0.32 | 0.94 | 0.40 | 44 |
| | | | 0.32 | 1.30 | 0.40 | 56 |
| $(Et_4N)_3[MoFe_3S_4(S\text{-}p\text{-}C_6H_4Cl)_3((al)_2cat)(EtCN)]$ (7) | | | | | | |
| solid | 5.12 | 4.2 | 0.42 | 0.91 | 0.40 | 68 |
| | | | 0.40 | 2.25 | 0.37 | 32 |
| MeCN soln | 4.99 | | ... | ... | ... | ... |
| $(Et_4N)_4[Mo_2Fe_6S_8(S\text{-}p\text{-}C_6H_4Cl)_6((al)_2cat)_2]$ (4) | | | | | | |
| solid | ... | 4.2 | 0.28 | 1.41 | 0.26 | 62 |
| | | | 0.34 | 1.10 | 0.28 | 38 |

[a] At ~297 K; $\mu_{eff} = 2.828(\chi_M T)^{1/2}\mu_B$. [b] ±0.03 mm/s; relative to Fe metal at 4.2 K. [c] ±0.05 mm/s. [d] Line width at half-height. [e] Relative intensity (area) of quadrupole doublet.

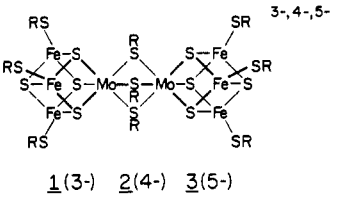


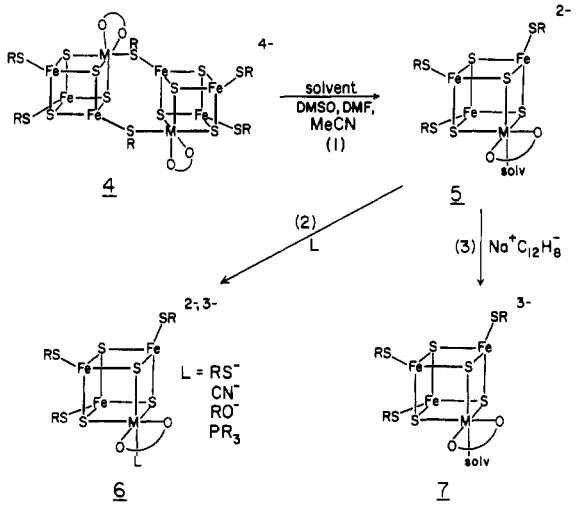


**Figure 1.** Schematic structural formulas of triply bridged (**1–3**), doubly bridged (**4**), and single cubanes (**5–7**) and reactions 1–3, which lead to the formation of **5–7** from **4**.

$$[Mo_2Fe_6S_8(SR)_9]^{3-} \underset{-e^-}{\overset{+e^-}{\rightleftharpoons}} [Mo_2Fe_6S_8(SR)_9]^{4-} \underset{-e^-}{\overset{+e^-}{\rightleftharpoons}} [Mo_2Fe_6S_8(SR)_9]^{5-} \quad (4)$$
$$\mathbf{1}\ (2\alpha) \qquad \mathbf{2}\ (\alpha+\beta) \qquad \mathbf{3}\ (2\beta)$$

$$[MoFe_3S_4(SR)_3(3,6\text{-}R'_2cat)(solv)]^{2-} \underset{-e^-}{\overset{+e^-}{\rightleftharpoons}} [MoFe_3S_4(SR)_3(3,6\text{-}R'_2cat)(solv)]^{3-} \quad (5)$$
$$\mathbf{5}\ (\alpha) \qquad \mathbf{7}\ (\beta)$$

(**6**; L = $p$-$ClC_6H_4S^-$, M = Mo; L = CN, M = Mo, W).[12] Catecholate ligands are designated by $Pr_2$cat (3,6-di-$n$-propylcatecholate) and $(al)_2$cat (3,6-diallylcatecholate). The solvated clusters **5** were generated in solution by reaction 1. The reduced solvated cluster salt $(Et_4N)_3[MoFe_3S_4(S\text{-}p\text{-}C_6H_4Cl)_3((al)_2cat)(EtCN)]$ (**7**, solv = EtCN) was prepared by reaction 3; details of the synthesis are reported elsewhere.[16]

**Physical Measurements.** Magnetic susceptibilities of solid and solution samples at ambient temperature were determined by the Faraday ($HgCo(NCS)_4$ calibrant) and $^1H$ NMR[20] ($Me_4Si$ reference) methods, respectively. Solvent susceptibility[21] and diamagnetic corrections[22] were taken from published data. EPR spectra were determined at X-band frequencies with a Varian E-109 spectrometer equipped with a Helitran Model LTD-3-110 temperature controller. Mössbauer spectral measurements were made with a conventional constant-acceleration spectrometer equipped with a $^{57}Co$ source in a rhodium matrix maintained at the same temperatures as the absorber. Spectra were measured in zero applied magnetic field at various temperatures and in longitudinally applied fields up to 80 kOe at 4.2 K. Polycrystalline and solution samples were prepared as previously described.[23] Cluster concentrations in solution samples were ~30 mM. Magnetization measurements of solid samples were carried out at 1.43 and 4.2 K over an external magnetic field range of 0–90 kOe with a vibrating-sample magnetometer[24] adapted to a superconducting solenoid. Samples of ca. 20–30 mg were measured in thin-walled Delrin or Kel-F containers. All measurements were performed under strictly anaerobic conditions.

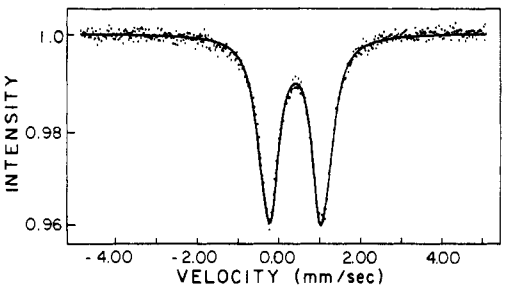


**Figure 2.** Mössbauer spectrum of polycrystalline $(Et_4N)_3[MoFe_3S_4(S\text{-}p\text{-}C_6H_4Cl)_4((al)_2cat)]$ (**6**) at 120 K. The solid line is a theoretical least-squares fit to the data assuming two inequivalent Fe sites and based on the parameters in Table I.

## Results and Discussion

Electronic properties of the single cubanes **6** and **7** and the doubly bridged double cubane **4** as manifested in $^{57}Fe$ Mössbauer spectra and low-temperature magnetization behavior are considered in the following sections. Mössbauer parameters based on two-site fits of experimental spectra and magnetic moments at ambient temperature are collected in Table I. All isomer shifts are referenced to Fe metal at the same temperature as the absorber.

**$[MoFe_3S_4(S\text{-}p\text{-}C_6H_4Cl)_4((al)_2cat)]^{3-}$ (6).** The Mössbauer

(20) Phillips, W. D.; Poe, M. *Methods Enzymol.* **1972**, *24*, 304.
(21) Gerger, W.; Mayer, U.; Gutmann, V. *Monatsh. Chem.* **1977**, 417.
(22) Mulay, L. N. In "Physical Methods of Chemistry"; Weissberger, A., Rossiter, B. W., Eds.; Wiley-Interscience: New York, 1972; Part IV, Chapter VII.
(23) Laskowski, E. J.; Reynolds, J. G.; Frankel, R. B.; Foner, S.; Papaefthymiou, G. C.; Holm, R. H. *J. Am. Chem. Soc.* **1979**, *101*, 6562.
(24) Foner, S. *Rev. Sci. Instrum.* **1959**, *30*, 548.

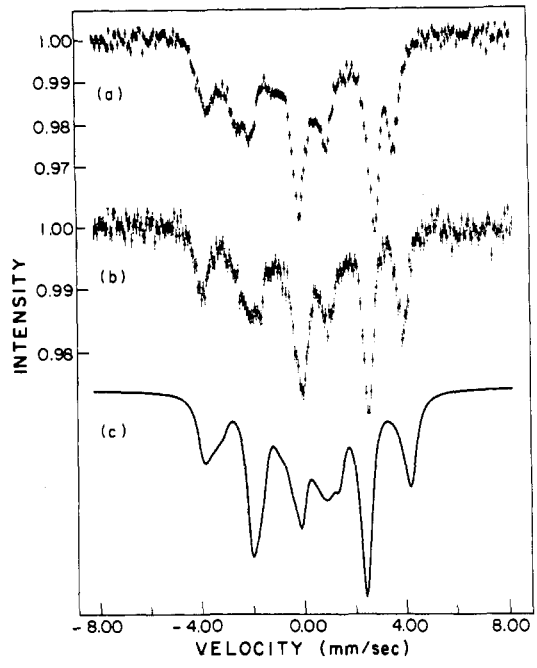


**Figure 3.** Mössbauer spectra of polycrystalline $(Et_4N)_3[MoFe_3S_4(S\text{-}p\text{-}C_6H_4Cl)_4((al)_2cat)]$ (**6**) at 4.2 K in longitudinal magnetic fields of (a) 60 kOe and (b) 80 kOe. The solid line (c) is a theoretical simulation of spectrum b assuming two magnetic subsites with intensity ratio 2:1.

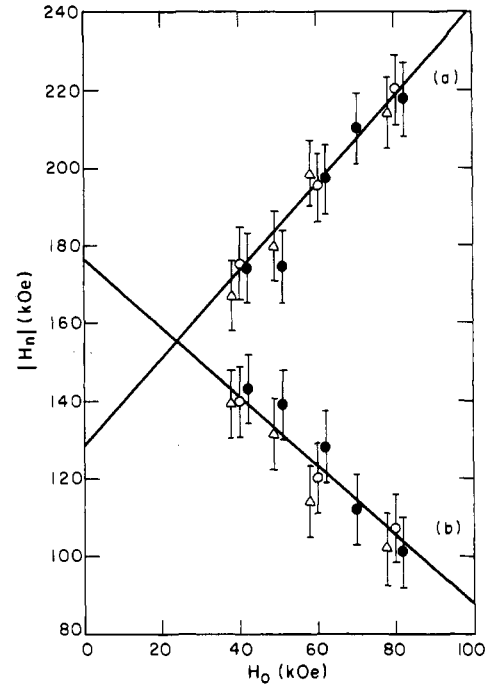


**Figure 4.** Total magnetic field at the nucleus $H_n$ in $(Et_4N)_3[MoFe_3S_4(S\text{-}p\text{-}C_6H_4Cl)_4((al)_2cat)]$ (**6**) as a function of the applied field $H_0$: (○) polycrystalline sample; (●, △) two different acetonitrile solution samples. Lines a and b refer to the less intense and more intense subsites, respectively.

spectrum of the polycrystalline $Et_4N^+$ salt, shown in Figure 2, consists of an apparent quadrupole doublet with isomer shift $\delta = 0.30 \pm 0.03$ mm/s and quadrupole splitting $\Delta E_Q = 1.31 \pm 0.06$ mm/s. However, the relatively broad line width ($\Gamma = 0.56$ mm/s) implies inequivalence of the Fe sites in **6**. The ambient-temperature crystal structure of the compound contains a cluster that approaches $C_s$ symmetry.[11,12] In idealized $C_s$ symmetry, the highest possible for the cluster owing to the presence of the catecholate chelate ring at the Mo atom,[25] two Fe atoms are related by the mirror plane that bisects the ring and contains Mo, Fe, and two S atoms. The spectrum was satisfactorily fit with two quadrupole doublets of narrower line widths and constrained in a 2:1 intensity ratio. The doublets in this and the 80 K spectrum differ primarily in their quadrupole splittings. In fluid acetonitrile solution at ambient temperature the $^1H$ NMR spectrum of **6** is consistent with $C_s$ symmetry, a property of all ligated clusters.[11,12] Because the exact structure in solution is unknown, two-site fits were also investigated but the relative intensities of the doublets were left as a free parameter. Best fits of frozen-solution spectra at 80 and 130 K yielded isomer shifts essentially indistinguishable from those in the solid state but smaller quadrupole splittings. Previously we have introduced the *empirical* relationship (6) between isomer shift and (mean) oxidation state

$$\delta = 1.44 - 0.43s \qquad (6)$$

$s$ of an Fe atom in a tetrahedral $S_4$ site.[14] The equality of, or very small differences in, $\delta$ values for the subsites of **6** in the solid and solution phases shows that the $\alpha$ oxidation level is electronically delocalized, with the mean oxidation state approximation $Fe^{2.67+}$ following from eq 6.

Incipient hyperfine interactions arising from the paramagnetism of the cluster result in additional line broadening and an asymmetry in the spectrum of **6** at $T \lesssim 80$ K (not shown). At 4.2 K the lower energy absorption feature is broader, indicating negative signs of the principal components of the electric field gradient (efg) tensors.

Application of an external magnetic field at 4.2 K results in induced magnetic hyperfine splittings in addition to the splittings due to the applied field. Spectra at $H_0 = 60$ and 80 kOe and 4.2 K for the polycrystalline $Et_4N^+$ salt of **6** are presented in Figure 3. At least two magnetic subsites with 2:1 relative intensities are resolved. Splittings of the features of the more and less intense subsites decrease and increase, respectively, with increasing $H_0$. This behavior is indicative of antiparallel exchange coupling of the Fe spins in the cluster, such as has been observed in, e.g., the ferredoxin site analogues $[Fe_4S_4(SR)_4]^{3-}$.[23,26,27] The more intense subsite is associated with the negative hyperfine field corresponding to the majority spins. The magnetically perturbed spectra were simulated with the assumption of two magnetic subsites. Quadrupole splittings and isomer shifts were taken from the zero-field spectral fits, and the angle between the principal component of the efg tensor and the magnetic field was averaged, as required for a powder sample. For simplicity the efg tensor was assumed to be symmetric (asymmetry parameter $\eta = 0$). Comparison of the simulated spectra with the data allows an estimate of the total magnetic field $H_n$ for the subsites at each value of $H_0$. These are plotted in Figure 4 for **6** in the polycrystalline and solution states. The total field at the nucleus in subsite $i$ is given by eq 7. If the induced spin and hence the hyperfine

$$\vec{H}_{n_i} = \vec{H}_0 + \vec{H}_{\mathrm{hf}_i} \qquad (7)$$

field $H_{hf}$ are parallel to $H_0$, eq 7 becomes a scalar equation and $H_{hf_i}$ can be determined from the intercepts of the plots in Figure 4. This procedure gives −176 and +128 kOe for the more and less intense subsites, respectively.

Magnetization data for **6** in the polycrystalline state at 1.43 and 4.2 K in applied fields up to 55 kOe are presented in Figure 5. The saturation magnetic moment $\mu_{sat} \simeq 3\ \mu_B$ at

(25) Crystallographically imposed $C_s$ symmetry is found in the structure of the $Et_4N^+$ salt of the closely related cluster $[MoFe_3S_4Cl_3((al)_2cat)(THF)]^{2-}$.[13]

(26) Lane, R. W.; Wedd, A. G.; Gillum, W. O.; Laskowski, E. J.; Holm, R. H.; Frankel, R. B.; Papaefthymiou, G. C. *J. Am. Chem. Soc.* **1977**, *99*, 2350.
(27) Stephan, D. W.; Papaefthymiou, G. C.; Frankel, R. B.; Holm, R. H. *Inorg. Chem.* **1983**, *22*, 1550.

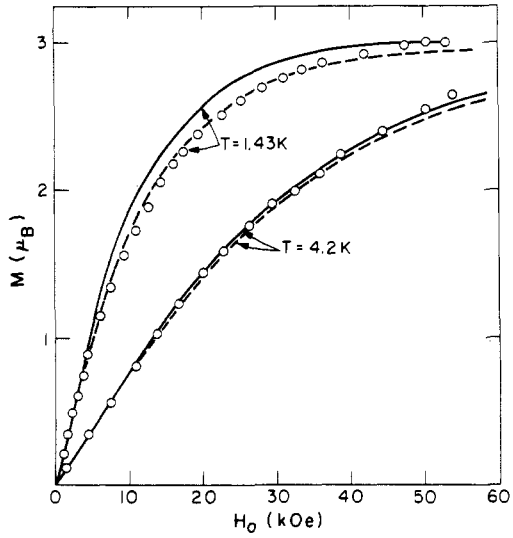


**Figure 5.** Magnetization of polycrystalline $(Et_4N)_3[MoFe_3S_4(S\text{-}p\text{-}C_6H_4Cl)_4((al)_2cat)]$ (**6**) at 1.43 and 4.2 K as a function of the applied field $H_0$. The solid and dashed lines are theoretical simulations with $D = E = 0$ and $D = \pm 1$ cm$^{-1}$, $E = 0$, respectively.

the lower temperature confirms the $S = {}^3/_2$ ground state of the cluster. At 4.2 K the saturation limit is not achieved. Effective magnetic moments of **6** in the solid and solution states at ambient temperature (Table I) are slightly larger than the spin-only moment of 3.87 $\mu_B$ but are consistent with a quartet ground state. All single cubanes **5** and **6** with the $\alpha$ oxidation level have $\mu_{eff} = 3.9$–$4.1$ $\mu_B$ at ambient temperature.[9-12] The magnetization results were analyzed with use of the spin Hamiltonian (8) where $D$ and $E$ are the axial and rhombic

$$H_e = D[S_z^2 - {}^1/_3S(S+1)] + E(S_x^2 - S_y^2) + g_e\mu_B\vec{H}\cdot\vec{S} \quad (8)$$

zero-field splitting parameters, $g_e$ is the electronic $g$ value, and $\mu_B$ is the Bohr magneton. Reasonable simulations were achieved with $E = 0$ and $D = 0, \pm 1$ cm$^{-1}$ (Figure 5). A more accurate value of $D$ could not be obtained by this method because the simulations for a powder sample are not sensitive to small values of $D$.[28]

The hyperfine field is related to the induced spin by eq 9,

$$H_{hf_i} = -A_{0_i}\langle S\rangle / g_n{}^*\mu_n \quad (9)$$

where $A_{0_i}$ is the magnetic hyperfine coupling constant for subsite $i$, $\langle S\rangle$ is the expectation value of the electron spin, $g_n{}^*$ is the nuclear $g$ value of the 14.4-keV level of $^{57}$Fe, and $\mu_n$ is the nuclear magneton. Because of the small value of $D$, $\langle\vec{S}\rangle \cong {}^3/_2$ when $H_0 \lesssim 30$ kOe. With use of the experimental values of $H_{hf}$, $A_0 = 4.6 \times 10^{-4}$ cm$^{-1}$ and $-3.5 \times 10^{-4}$ cm$^{-1}$ for the more intense and less intense subsites, respectively.

**$[MoFe_3S_4(S\text{-}p\text{-}C_6H_4Cl)_3((al)_2cat)(EtCN)]^{3-}$ (7).** The $Et_4N^+$ salt of this cluster is the only reduced single cubane thus far isolated.[16] Its crystal structure has not been determined, but its $^1$H NMR spectrum and that of its $PEt_3$ adduct are consistent with the solvated description **7** and a ligated structure analogous to **6**,[12] respectively. The Mössbauer spectrum of the polycrystalline compound at 4.2–200 K consists of two well-resolved quadrupole doublets. The 4.2 K spectrum is shown in Figure 6 together with a theoretical least-squares fit based on two subsites. The doublets have relative intensities that are very close to 2:1. The larger quadrupole splitting is

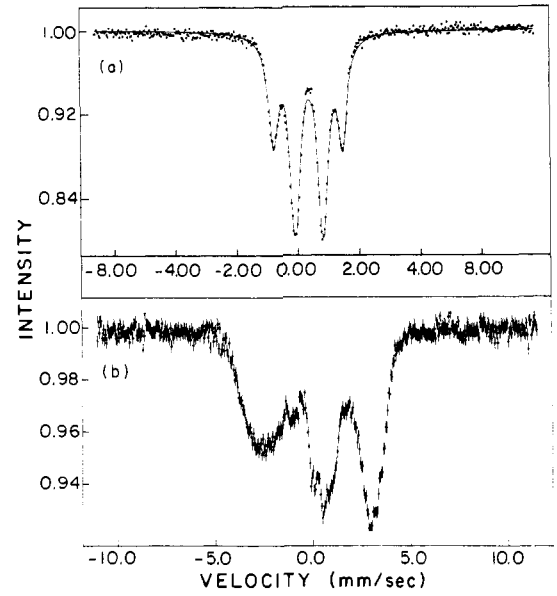


**Figure 6.** Mössbauer spectra of polycrystalline $(Et_4N)_3[MoFe_3S_4(S\text{-}p\text{-}C_6H_4Cl)_3((al)_2cat)(EtCN)]$ (**7**) at 4.2 K and (a) $H_0 = 0$ and (b) $H_0 = 80$ kOe. The solid line in (a) is a theoretical least-squares fit to the data assuming two inequivalent Fe sites and based on the parameters in Table I.

a property of the less intense subsite. That the subsite isomer shifts are indistinguishable demonstrates substantial electron delocalization in the $\beta$ oxidation level. From eq 6 with $\delta = 0.41$ mm/s it is found that $s = 2.40$, a value interpreted as the mean oxidation state $Fe^{2.33+}$.

As with **6**, application of an external field at 4.2 K results in induced magnetic hyperfine splittings in addition to the splittings produced by $H_0$. The spectrum of **7** at $H_0 = 80$ kOe is included in Figure 6; the overall splitting is comparable to that in the 80-kOe spectrum of **6**. Clearly distinct magnetic subsites are not seen in the high-field spectrum. However, the presence of induced hyperfine fields requires a paramagnetic ground state. The ambient-temperature magnetic moments $\mu_{eff} = 5.12$ $\mu_B$ (solid) and 4.99 $\mu_B$ (solution) are consistent with a $S = 2$ spin system, for which the spin-only value is 4.90 $\mu_B$.

The only other isolated cluster with the $\beta$ oxidation level is the fully reduced double cubane $[Mo_2Fe_6S_8(SPh)_9]^{5-}$ (**3**).[14] Its magnetic moment (4.84$\mu_B$/subcluster) and Mössbauer parameters[14] from a two-site fit of the 4.2 K spectrum ($\delta_1 = 0.42$, $\Delta E_{Q_1} = 0.84$, $\delta_2 = 0.41$, $\Delta E_{Q_2} = 2.21$ mm/s, solid state) are nearly identical with those of **7**. This situation provides confirmation of an earlier argument[14] that the ~2:1 intensity distribution of the doublets of **3** arises from sites within each subcluster rather than from some combination of inequivalent subclusters. While such a distribution is consistent with cluster $C_s$ symmetry, it is not evident why it should occur in the subclusters of **3**, where it persists in solid and solution samples at 4.2–130 K. The ambient-temperature structure of this species involves no imposed symmetry, but each subcluster is dominantly trigonal. Structural parameters do not permit a clear sorting of Fe sites into two types.

**$[Mo_2Fe_6S_8(S\text{-}p\text{-}C_6H_4Cl)_6((al)_2cat)_2]^{4-}$ (4).** As seen in Figure 7, the Mössbauer spectrum of the polycrystalline $Et_4N^+$ salt of **4** consists of two overlapping quadrupole doublets. The spectrum was satisfactorily fit with two doublets in a ~2:1 intensity ratio with a 0.06 mm/s difference in isomer shifts. From the ambient-temperature structures of the triclinic and monoclinic forms of the compound,[9] each subcluster including the catecholate chelate ring approaches $C_s$ symmetry. Consequently, it is probable that the less intense subsite is that Fe atom involved in the Fe–(SR)–Mo bridge unit. As is the case for **6**, the small differences in isomer shifts reflect a

(28) For large axial distortions which result in the orientation of $\langle\vec{S}\rangle$ in a preferred plane, the shapes of the magnetization curves are much more sensitive to the value of $D$. For an example, cf.: Papaefthymiou, G. C.; Frankel, R. B.; Foner, S.; Tang, S. C.; Koch, S.; Holm, R. H. *J. Phys. (Orsay, Fr.)* **1976**, *37*, C6-209.

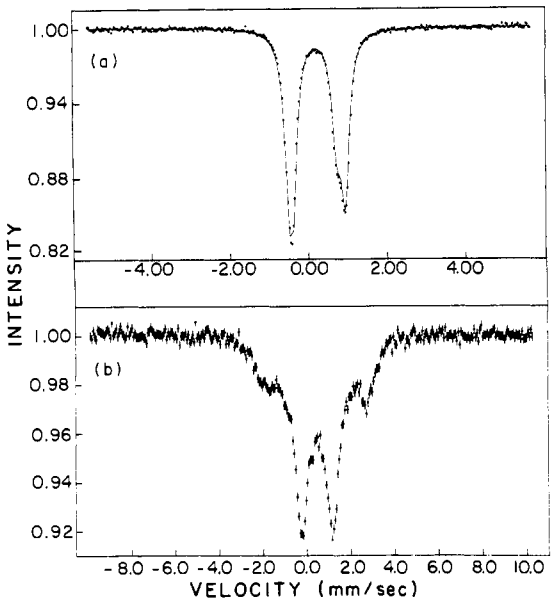


**Figure 7.** Mössbauer spectra of polycrystalline $(Et_4N)_4[Mo_2Fe_6S_8(S\text{-}p\text{-}C_6H_4Cl)_6((al)_2cat)_2]$ (**4**) at 4.2 K and (a) $H_0 = 0$ and (b) $H_0 = 80$ kOe. The solid line in (a) is a theoretical least-squares fit to the data assuming two inequivalent Fe sites and based on the parameters in Table I.

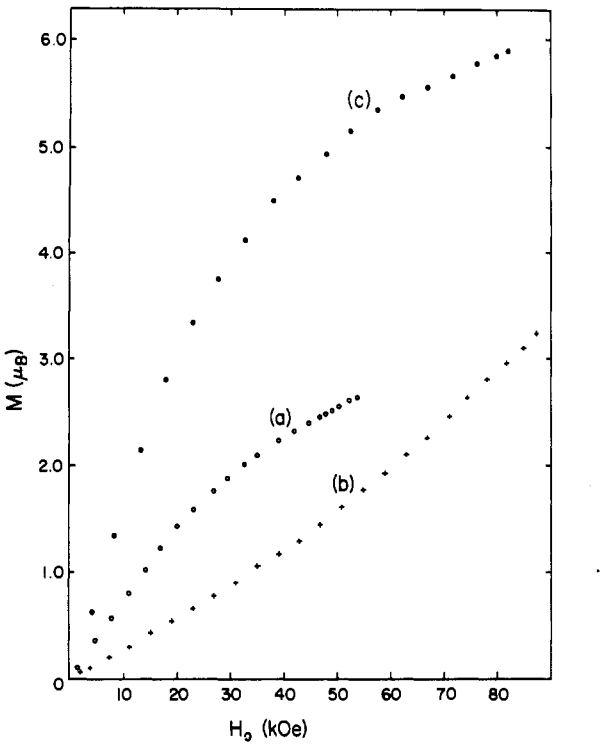


**Figure 8.** Magnetization per cluster anion of polycrystalline (a) $(Et_4N)_3[MoFe_3S_4(S\text{-}p\text{-}C_6H_4Cl)_4((al)_2cat)]$ (**6**), (b) $(Et_4N)_4[Mo_2Fe_6S_8(S\text{-}p\text{-}C_6H_4Cl)_6((al)_2cat)_2]$ (**4**), and (c) $(Et_4N)_3[Mo_2Fe_6S_8(S\text{-}p\text{-}C_6H_4Cl)_9]$ (**1**) as a function of applied magnetic field at 4.2 K.

delocalized structure of the $\alpha$ oxidation level and the average $\delta$ value of 0.30 mm/s indicates the mean oxidation state $Fe^{2.67+}$.

Application of an external magnetic field results in a Mössbauer spectrum of **4** that is very different from that of **6**. The 80-kOe spectrum in Figure 7 (compare with Figure 3) originates from two magnetic subsites with ~2:1 relative intensity. The splitting of the two lines of the more intense subsite is nearly field invariant whereas that of the less intense subsite increases with increasing field. Together with magnetization results (vide infra) the spectrum is interpreted in terms of antiparallel coupling of the net spins of the two $\alpha$ subclusters to produce a singlet ground state and low-lying paramagnetic state(s). The states are mixed by the applied field to give a Van Vleck type paramagnetic moment which increases with increasing field. From spectra at different $H_0$ values it is estimated that for the more intense subsite $H_{hf} = -H_0$, resulting in $H_n = 0$. For the less intense subsite the hyperfine field is smaller and oppositely signed, i.e., $H_{hf} = aH_0$ ($a \cong 0.5$), giving $H_n = (1 + a)H_0$. This implies antiparallel spin coupling between Fe atoms in each subcluster.

The magnetization behavior of **4** in the solid state at 4.2 K, displayed in Figure 8, is essentially linear with $H_0$ up to about 40 kOe. At $40 \lesssim H_0 \lesssim 90$ kOe positive deviations from extrapolation of the linear region are observed. The moment at constant field is temperature independent below 4.2 K but increases at higher temperatures, with a maximum between 6 and 10 K (not shown). These results are indicative of a singlet ground state and an excited paramagnetic state. The increase in moment above ~40 kOe at 4.2 K signals the approach (and population) of components of the excited state (possibly $S = 1$) to the singlet level at these high fields.

For purpose of comparison the magnetization of polycrystalline $(Et_4N)_3[Mo_2Fe_6S_8(S\text{-}p\text{-}C_6H_4Cl)_9]$, a triply bridged double cubane of type **1**, is included in Figure 8. Unlike the doubly bridged double cubane **4** the moment approaches saturation at $H_0 \approx 80$ kOe. The saturation moment is clearly very close to 6 $\mu_B$/anion or 3 $\mu_B$/subcluster, in agreement with magnetic susceptibility results near 300 K for other $[Mo_2Fe_6S_8(SR)_9]^{3-}$ and $[Mo_2Fe_6S_8(OMe)_3(SR)_6]^{3-}$ clusters, which accord with a net spin $S = {}^3/_2$ per subcluster.[14,17] The value of 3 $\mu_B$ is the same as the saturation moment of the single cubane **6**, an expected result since both species have the $\alpha$ oxidation level. Inasmuch as the subclusters of **4** also have this oxidation level, the major electronic difference between doubly bridged **4** and triply bridged **1** is the strength of the exchange coupling between subclusters. This interaction clearly is larger in **4**.

**Summary.** A substantial body of information on the electronic properties of $MoFe_3S_4$ clusters of the single-[8-12] and double-cubane[2,3,6,14-17,29] types has now been collected. The following is a summary of the status of interpretation of certain leading electronic features of these clusters.

**(1) Spin Ground States.** Low-temperature magnetization data are conclusive in establishing the $S = {}^3/_2$ state for $[MoFe_3S_4(S\text{-}p\text{-}C_6H_4Cl)_4((al)_2cat)]^{3-}$ (**6**) and the subclusters of $[Mo_2Fe_6S_8(S\text{-}p\text{-}C_6H_4Cl)_9]^{3-}$ (**1**). Ambient-temperature magnetic moments of these and other clusters of types **1**,[6,14,17,29] **5**,[9,10] and **6**[11,12] are consistent with a quartet state as are the EPR spectra of **5** and **6** (vide infra). It is probable that this state applies to all clusters with the $\alpha$ ($[MoFe_3S_4]^{3+}$) oxidation level, including the subclusters of $[Mo_2Fe_6S_8(S\text{-}p\text{-}C_6H_4Cl)_6((al)_2cat)_2]^{4-}$ (**4**). In this doubly bridged double-cubane subcluster net spins appear to be more strongly coupled than in the triply bridged double cubanes **1**[17] (Figure 8), resulting in a $S = 0$ ground state. One-electron reduction of $\alpha$ clusters to the $\beta$ ($[MoFe_3S_4]^{2+}$) oxidation level, as in series 4 and 5, has thus far afforded two isolable species, $[Mo_2Fe_6S_8(SPh)_9]^{5-}$ (**3**)[14] and $[MoFe_3S_4(S\text{-}p\text{-}C_6H_4Cl)_3((al)_2cat)(EtCN)]^{3-}$ (**7**), whose ambient-temperature magnetic moments are consistent with $S = 2$ states. Magnetization data for $\beta$ clusters are not available.

**(2) Charge Distribution.** The isomer shift data for clusters **4** and **6** (Table I), when compared with those for clusters **1** and $[Mo_2Fe_6S_8(OMe)_3(SPh)_6]^{3-}$,[2,14,15] demonstrate that mean $\delta$ values of $\alpha$ clusters are not significantly dependent on bridge structure or its presence. The most important result for these

(29) Christou, G.; Collison, D.; Garner, C. D.; Mabbs, F. E.; Petrouleas, V. *Inorg. Nucl. Chem. Lett.* **1981**, *17*, 137.

clusters is that isomer shifts are sensibly consistent only with mean fractional Fe oxidation states; i.e., the $Fe_3$ cluster portions are electronically delocalized to about the same extent independent of different structural features at the Mo site. Reduction to the $\beta$ oxidation level affords an increase in mean $\delta$ values of **3** and **7** to 0.41 mm/s in the solid state at 4.2 K. These changes of 0.10–0.11 mm/s may be compared with 0.14 mm/s calculated from eq 6 if the added electron density is assumed to be equally divided over the three Fe sites. This comparison provides reasonable evidence that the $Fe_3$ portions of the $\alpha$ and $\beta$ clusters are those primarily affected by the redox process. Potentials of the steps in series 4[14,15] and 5[9] parallel those of $[Fe_4S_4(SR)_4]^{2-,3-}$ couples (R constant), supporting the qualitative view that orbitals involved in electron gain and loss are heavily Fe–S in character.

A subsidiary issue is the exact description of the mean Fe oxidation state in $\alpha$ and $\beta$ clusters. For the former we have favored $Fe^{2.67+}$ [2,14,18] (i, $2Fe^{3+} + Fe^{2+} + Mo^{3+}$), on the basis of eq 6, which provides the only means of estimating, directly from experimental data, oxidation states of Fe atoms in sites structurally similar to those in $MoFe_3S_4$ clusters. Because of the empirical nature of the approach we do not insist upon the stated description, the alternative to which is $Fe^{2.33+}$ (ii, $Fe^{3+} + 2Fe^{2+} + Mo^{4+}$). Magnetic Mössbauer spectra confirm antiparallel spin coupling between two Fe subsites, and the net $S = 3/2$ spin is derivable with use of either description. Given that the principal locus of reduction is the $Fe_3$ portion, the isomer shifts of clusters appear to accord somewhat less well with the reduced version of state ii ($3Fe^{2+} + Mo^{4+}$) than of state i ($Fe^{2.33+}$). Isomer shifts of tetrahedral $Fe^{II}S_4$ units at 4.2 K tend to be 0.5–0.6 mm/s[30–33] and are usually at the high end of the range.[34] A recent theoretical analysis of the bulk susceptibilities of triply bridged double cubanes containing $\alpha$ clusters did not permit a distinction between subcluster coupling schemes based on states i and ii.[17]

**(3) Isotropic NMR Shifts.** $^1H$ and some $^{19}F$ NMR spectra have been reported for examples of clusters **1**–**3**[3,4,6,14] and **5**–**7**.[8–13] The existence of dominant hyperfine contact interactions at the Fe sites effected by ligand → metal antiparallel spin delocalization is supported by relative signs of arenethiolate proton, F, $CH_3$, and $CF_3$ shifts, near-coincidence of the temperature dependence of normalized shifts and susceptibilities of $\alpha$ clusters, and increased shifts upon passing from $\alpha$ ($S = {}^3/_2$) to the more paramagnetic $\beta$ ($S = 2$) clusters. These properties as diagnostic of contact shifts are discussed elsewhere.[36] The last property is represented by eq 10, in

$$\frac{(\Delta H/H_0)_\alpha^{con}}{(\Delta H/H_0)_\beta^{con}} = \frac{A_\alpha \mu_\alpha^2}{A_\beta \mu_\beta^2} \qquad (10)$$

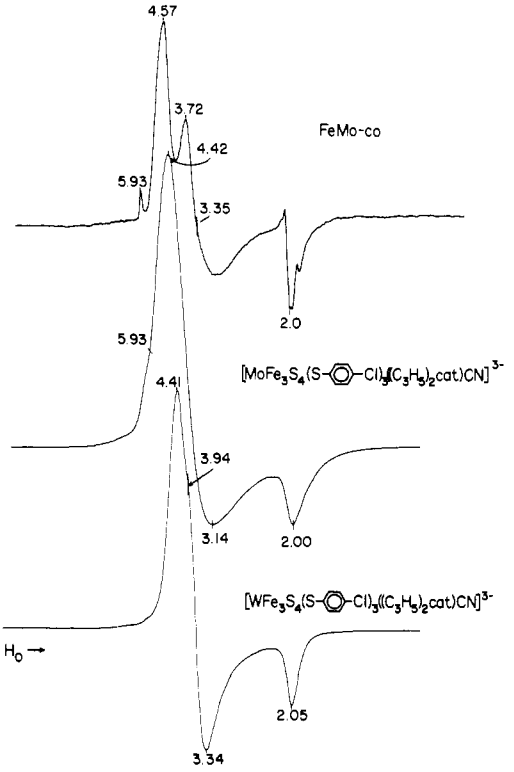


**Figure 9.** EPR spectra (X band) of FeMo-co (1.4 mM Mo) from *Azotobacter vinelandii* Fe protein in *N*-methylformamide and 10 mM $[MFe_3S_4(S\text{-}p\text{-}C_6H_4Cl)_3((al)_2cat)CN]^{3-}$ (M = Mo, W) in acetonitrile at ~7 K. All spectra were recorded at 5-mW microwave power; 10-G and 40-G modulation amplitudes were used in the upper spectrum and lower two spectra, respectively. Selected $g$ values are indicated.

which the $A$ values are coupling constants of a given nucleus in the two oxidation levels. In acetonitrile at 297 K the isotropic shifts and squared magnetic moment ratios are 1.52 and 1.50, respectively, for $[MoFe_3S_4(S\text{-}p\text{-}C_6H_4Cl)_3((al)_2cat)(MeCN)]^{2-}$ (**5**) and **7**.[37] Thus the ratio $A_\alpha/A_\beta \cong 1$, a reasonable result for two species with pure contact shifts produced by the same delocalization mechanism. Isotropic shifts of Mo-bound ligands are also found in the clusters **5** and **6**. Those of L = arenethiolates are very small ($\lesssim$1 ppm), but those of catecholate ring protons can be as large as ~+5 ppm and vary from −3 to +4 ppm in $\alpha$ and $\beta$ clusters, respectively, at ambient temperature. Shifts in both oxidation levels vary with solvent and ligand L.[9,10,12] The contact and dipolar contributions to these shifts are unknown.

**(4) EPR Spectra.** Spectra of double cubanes of types **1**[17] and **4**[8] in the solid state are complex, presumably because of weak subcluster coupling. The powder spectrum of $[W_2Fe_6S_8(OMe)_3(SPh)_6]^{3-}$ as well as the temperature dependence of its magnetic susceptibility are best simulated by using a theoretical model including such an interaction.[17] The spectra of the single cubanes **5** and **6**, several examples of which have been presented earlier,[9,11,12] are substantially simpler and are consistent with a $S = {}^3/_2$ spin system with a small rhombic distortion in both solid and solution phases. The solution spectrum of $[MoFe_3S_4(S\text{-}p\text{-}C_6H_4Cl)_3((al)_2cat)CN]^{3-}$ (**6**, L = $CN^-$; 4.09 $\mu_B$ at 295 K), shown in Figure 9 with that of its tungsten analogue, is typical. Spectra of single cubanes are best observed at $T \lesssim 15$ K because of rapid electron spin relaxation. For example, the peak height of the $g \approx 4.4$ feature of 10 mM $[MoFe_3S_4(SPh)_3(Pr_2cat)(Me_2SO)]^{2-}$ in $Me_2SO$

(30) Simopoulos, A.; Papaefthymiou, V.; Kostikas, A.; Petrouleas, V.; Coucouvanis, D.; Simhon, E. D.; Stremple, P. *Chem. Phys. Lett.* **1981**, *81*, 261.
(31) Coucouvanis, D.; Stremple, P.; Simhon, E. D.; Swenson, D.; Baenziger, N. C.; Draganjac, M.; Chan, L. T.; Simopoulos, A.; Papaefthymiou, V.; Kostikas, A.; Petrouleas, V. *Inorg. Chem.* **1983**, *22*, 293.
(32) Mascharak, P. K.; Papaefthymiou, G. C.; Frankel, R. B.; Holm, R. H. *J. Am. Chem. Soc.* **1981**, *103*, 6110.
(33) Bearwood, P.; Gibson, J. F.; Johnson, C. E.; Rush, J. D. *J. Chem. Soc., Dalton Trans.* **1982**, 2015.
(34) The correlation of eq 6 is based on data for well-defined Fe–S compounds, and as already stated,[14] it may be perturbed by the presence of a Mo atom within bonding distance. A possible case in point is the nominal Fe(II)–Mo(VI) dimer $[(PhS)_2FeS_2MoS_2]^{2-}$, whose isomer shift of 0.32–0.33 mm/s at 4.2–77 K[30,31,35] gives "$Fe^{2.6+}$" from eq 6. Difficulties with this interpretation have been noted.[35] While it seems unlikely that Mo(III or IV) at a comparable distance (~2.7 Å) from three Fe atoms could cause all three to appear significantly more oxidized than $Fe^{2+}$, were this the most physically meaningful oxidation-state designation, the matter remains open.
(35) Tieckelmann, R. H.; Silvis, H. C.; Kent, T. A.; Huynh, B. H.; Waszczak, J. V.; Teo, B.-K.; Averill, B. A. *J. Am. Chem. Soc.* **1980**, *102*, 5550.
(36) Reynolds, J. G.; Laskowski, E. J.; Holm, R. H. *J. Am. Chem. Soc.* **1978**, *100*, 5315 and references therein.
(37) Isotropic shifts of *m*-H: −9.17 (**7**), −6.04 (**5**) ppm. Magnetic moments ($\mu_{eff}$): 4.99 (**7**), 4.08 (**5**) $\mu_B$.

Table II. Comparative Electronic Properties of Synthetic and Native Mo-Fe-S Clusters

| property | synthetic | native[a] | ref |
|---|---|---|---|
| ground state $S$ | $^3/_2$ ($\alpha$), 2 ($\beta$) | $^3/_2$, $\geq 1$ (integer, red. form[b]) | *c*, 10, 38, 44 |
| $\delta_{av}$, mm/s[d] | 0.28–0.32 ($\alpha$) | 0.25, 0.28–0.29[b] | *c*, 2, 14, 44–47 |
| | 0.40–0.42 ($\beta$) | 0.34 (0.24) | *c*, 46 |
| $A_0$, $cm^{-1}$ | $4.6 \times 10^{-4}$, $-3.5 \times 10^{-4}$ ($\alpha$) | $(3.7\text{–}5.6) \times 10^{-4}$ $-3.1 \times 10^{-4}$ | *c*, 46 |
| $g$ values | 4.4–4.6, ~3.5,[e] $\lesssim$2.0$\|\pm^1/_2\rangle$, ~5.9$\|\pm^3/_2\rangle$ ($\alpha$) | 4.6, 3.3, $\lesssim$2.0$\|\pm^1/_2\rangle$, 5.9$\|\pm^3/_2\rangle$; 4.32, 3.65, 2.01,[b] $\|^1/_2\rangle$ | *c*, 9, 11, 12, 38, 44 |
| $D$, $cm^{-1}$ | ~0 to ±1 | ~+6[b] | *c*, 47 |
| $\lambda$[f] | ~0.08 | 0.11, 0.06[b] | *c*, 38 |
| hf broadening | | | |
| $^{95}Mo$ | none | none[b] | *c*, 38 |
| $^{57}Fe$ ($g \approx 2$) | small (~8%) | ~25% | |
| $(\Delta H/H_0)_{iso}$ ($^{19}F$, R = *p*-$C_6H_4F$, *p*-$C_6H_4CF_3$) | negative | negative | 10 |

[a] Refers to FeMo-co unless otherwise noted. [b] Fe protein(s). [c] This work. [d] At 4.2–80 K, values referenced to Fe metal at 4.2 K. [e] Unresolved. [f] $\Delta = 2D(1 + 3\lambda)^{1/2}$.[38]

solution at 11 K under nonsaturating power conditions is decreased by 79% at 58 K. At 80 K the spectrum is essentially unobservable.

On the basis of spin Hamiltonian (8) with $g_e = 2$ and $g\beta H << $ zero-field splitting, approximate expressions for the principal components of the **g** tensor of the $|\pm^1/_2\rangle$ and $|\pm^3/_2\rangle$ Kramers doublets of the $S = {}^3/_2$ system can be derived. Those for the $|\pm^1/_2\rangle$ doublet, given elsewhere,[38] lead to the assignments $g_y \approx 4.4\text{–}4.6$, $g_x \approx 3.5$, $g_z \lesssim 2$, and $|\lambda| \approx 0.08$ for all Mo single cubanes. In this treatment the zero-field splitting $\Delta = 2D(1 + 3\lambda^2)^{1/2}$, where $\lambda$ is an asymmetry parameter. The $g_x$ transition is not resolved because of the large line width (~450 G) of the $g \approx 4.4$ feature. A second feature, at $g \approx 3.9$, is just observable in the $g_\perp$ region of the tungsten cluster spectrum. The weak shoulder at $g \approx 5.9$, more evident in spectra of ligated than of solvated Mo clusters, is assigned to the forbidden $-^3/_2 \leftrightarrow +^3/_2$ transition in the other doublet. The nonzero value of $E$ apparent from the EPR spectra could not be established in fits of the magnetization data. Spectra of the solvated cluster $[MoFe_3S_4(SEt)_3(Pr_2cat)(Me_2SO)]^{2-}$, enriched separately to >95% in $^{95}Mo$ ($I = {}^5/_2$) and $^{57}Fe$ ($I = {}^1/_2$), were examined in $Me_2SO$ solutions at ~7 K. The unenriched and $^{95}Mo$ clusters gave identical spectra, but the $^{57}Fe$ cluster exhibited a signal at $g \approx 2$ whose half-width (380 G) is marginally (~8%) larger than that of the unenriched cluster. This observation conforms to the preceding Mössbauer and NMR spectral evidence of association of appreciable spin density with Fe atoms of $\alpha$ clusters.

**Comparison of Native and Synthetic Clusters.** The initial structural evidence for a native Mo–Fe–S cluster, present in Fe proteins of nitrogenase and extractable therefrom as FeMo-co,[39,40] was obtained from Mo EXAFS.[41,42] Recent Fe EXAFS[43] supports a cluster description. The structural similarities of Mo atom coordination sites in native and synthetic $MoFe_3S_4$ clusters have been described[18,19] and will be reported more fully elsewhere. Here we note briefly certain electronic similarities between the two types of clusters. Selected properties are compared in Table II, with emphasis on EPR and Mössbauer spectral results.[38,44–47] Some specific comments are in order. Both clusters exhibit antiparallel spin coupling as seen from oppositely signed $A_0$ values. The spin-quartet ground state of FeMo-co originally assigned from low-temperature EPR spectra is consistent with the ambient-temperature magnetic susceptibility.[10] The apparent Fe mean oxidation state of the native cluster in the $S = {}^3/_2$ state is comparable to (but perhaps slightly higher than) that of $\alpha$ clusters and indicates a delocalized structure. Subsites of the native cluster have been detected by Mössbauer[45–47] and ENDOR[48] spectroscopy; by the isomer shift criterion for $FeS_4$ units the subsites do not contain localized Fe(II,III). The EPR spectra of FeMo-co and one type **6** molybdenum cluster are directly compared in Figure 9. Despite the larger line widths of the synthetic species, a similarity is evident and extends to the appearance of a $g \approx 5.9$ weak resonance.[49] Comparison of $D$ values is limited to only one synthetic cluster. The negative isotropic shifts of *p*-F and *p*-$CF_3$ substitutents of arenethiolate ligands, which are bound to Fe in FeMo-co, are consistent with dominant contact interactions in the synthetic and native clusters.[10]

The foregoing results, together with EXAFS and X-ray structural information,[17,18] demonstrate the attainment of synthetic clusters, certain geometrical and electronic features of which approach those of the native Mo–Fe–S cluster of nitrogenase. On this basis research on the reactivity properties of $MoFe_3S_4$ species,[13] involving especially solvated clusters **5** and **7**, is under way in an attempt to develop substrate-reducing systems. Given the analytical Fe:S:Mo atom ratios of FeMo-co ((7–8):(8–9):1[39,40,50]) and a minimum of six Fe atoms coupled to the magnetic moment of the native cluster,[48] it is obvious that $MoFe_3S_4$ clusters are not analogues of the cofactor. However, the approach of properties provides continuing encouragement for exploratory synthesis aimed at the formation

(38) Münck, E.; Rhodes, H.; Orme-Johnson, W. H.; Davis, L. C.; Brill, W. J.; Shah, V. K. *Biochim. Biophys. Acta* **1975**, *400*, 32.
(39) Shah, V. K.; Brill, W. J. *Proc. Natl. Acad. Sci. U.S.A.* **1977**, *74*, 3249.
(40) Yang, S.-S.; Pan, W.-H.; Friesen, G. D.; Burgess, B. K.; Corbin, J. L.; Stiefel, E. I.; Newton, W. E. *J. Biol. Chem.* **1982**, *257*, 8042.
(41) Cramer, S. P.; Hodgson, K. O.; Gillum, W. O.; Mortenson, L. E. *J. Am. Chem. Soc.* **1978**, *100*, 3398.
(42) Cramer, S. P.; Gillum, W. O.; Hodgson, K. O.; Mortenson, L. E.; Stiefel, E. I.; Chisnell, J. R.; Brill, W. J.; Shah, V. K. *J. Am. Chem. Soc.* **1978**, *100*, 3814.
(43) Antonio, M. R.; Teo, B.-K.; Orme-Johnson, W. H.; Nelson, M. J.; Groh, S. E.; Lindahl, P. A.; Kauzlarich, S. M.; Averill, B. A. *J. Am. Chem. Soc.* **1982**, *104*, 4703.
(44) Rawlings, J.; Shah, V. K.; Chisnell, J. R.; Brill, W. J.; Zimmerman, R.; Münck, E.; Orme-Johnson, W. H. *J. Biol. Chem.* **1978**, *253*, 1004.
(45) Zimmermann, R.; Münck, E.; Brill, W. J.; Shah, V. K.; Henzl, M. T.; Rawlings, J.; Orme-Johnson, W. H. *Biochim. Biophys. Acta* **1978**, *537*, 185.
(46) Huynh, B. H.; Henzl, M. T.; Christner, J. A.; Zimmermann, R.; Orme-Johnson, W. H.; Münck, E. *Biochim. Biophys. Acta* **1980**, *623*, 124.
(47) Huynh, B. H.; Münck, E.; Orme-Johnson, W. H. *Biochim. Biophys. Acta* **1979**, *527*, 192.
(48) Hoffman, B. M.; Venters, R. A.; Roberts, J. E.; Nelson, M.; Orme-Johnson, W. H. *J. Am. Chem. Soc.* **1982**, *104*, 4711.
(49) Several other Mo–Fe–S complexes have $S = {}^3/_2$ ground states and EPR spectra similar to those of the native cluster: $[Fe(MoS_4)_2]^{3-}$[30] (McDonald, J. W.; Friesen, G. D.; Newton, W. E. *Inorg. Chim. Acta* **1980**, *46*, L79. Coucouvanis, D.; Simhon, E. D.; Baenziger, N. C. *J. Am. Chem. Soc.* **1980**, *102*, 6644) and $[(1,2\text{-}C_6H_4(CH_2S)_2)\text{-}FeS_2MoS_2]^{3-}$ (Friesen, G. D.; McDonald, J. W.; Newton, W. E. *Inorg. Chim. Acta* **1982**, *67*, L1).
(50) Nelson, M. J.; Levy, M. A.; Orme-Johnson, W. H. *Proc. Natl. Acad. Sci. U.S.A.* **1983**, *80*, 147.

of related delocalized clusters but with higher Fe:Mo ratios. Lastly, the set of electronic features now determined for $MoFe_3S_4$ clusters provides a meaningful test of any theoretical electronic structural model. One such model, based on the Xα approach, has been developed.[51]

**Acknowledgment.** This research was supported at Harvard University (Grant CHE 81-06017) and the Francis Bitter National Magnet Laboratory by the National Science Foundation. We thank Prof. D. Coucouvanis for a preprint of ref 31 and Dr. B. K. Burgess for a sample of FeMo-co.

**Registry No.** 1, 86645-74-1; 7, 86667-97-2; $[MoFe_3S_4(SEt)_3(Pr_2cat)(Me_2SO)]^{2-}$, 86645-75-2; $(Et_4N)_4[Mo_2Fe_6S_8(S\text{-}p\text{-}C_6H_4Cl)_6((al)_2cat)_2]$, 82247-34-5; $(Et_4N)_3[MoFe_3S_4(S\text{-}p\text{-}C_6H_4Cl)_4((al)_2cat)]$, 80789-40-8; $[MoFe_3S_4(S\text{-}p\text{-}C_6H_4Cl)_3((al)_2cat)CN]^{3-}$, 80702-97-2; $[WFe_3S_4(S\text{-}p\text{-}C_6H_4Cl)_3((al)_2cat)CN]^{3-}$, 84130-55-2; $[MoFe_3S_4(S\text{-}p\text{-}C_6H_4Cl)_3((al)_2cat)(MeCN)]^{2-}$, 80702-98-3; $[MoFe_3S_4(SPh)_3(Pr_2cat)(Me_2SO)]^{2-}$, 86645-76-3.

(51) Cook, M. D.; Karplus, M., manuscript in preparation.

Contribution from the Fachbereich Chemie der Phillips-Universität, D-3550 Marburg 1, West Germany

# $Cu^{2+}$ in Five-Coordination: A Case of a Second-Order Jahn-Teller Effect. 1. Structure and Spectroscopy of the Compounds $Cu(terpy)X_2 \cdot nH_2O$

W. HENKE, S. KREMER, and D. REINEN*

*Received December 29, 1982*

Five-coordinate $Cu^{2+}$ complexes were studied by means of ligand field and EPR spectroscopy in the compounds $Cu(terpy)X_2 \cdot nH_2O$ ($X = Cl^-, Br^-, I^-, NO_2^-, NO_3^-, F^-$). In addition single-crystal structure analyses of $Cu(terpy)Cl_2 \cdot nH_2O$ ($n = 0$, $P2_1/a$; $n = 1$, $C2/c$) were performed. The $CuN_3Cl_2$ polyhedra are essentially tetragonal pyramids, though the influence of the rigid tridentate terpy ligand leads to deviations from this geometry. The pyramids are strongly elongated with apical Cu-Cl spacings of ≃2.50 Å and relatively short equatorial bonds. Similar geometries are derived from the spectroscopic data of most of the cited compounds. Apparently the elongated tetragonal bipyramid is the favored geometry for five-coordinate $Cu^{2+}$ complexes of the considered constitution. In the EPR spectra of some compounds exchange coupling between $Cu^{2+}$ polyhedra of different orientations in the unit cell is observed. From the cooperative **g** tensors the molecular *g* values could be derived, with use of the crystallographic data.

## Introduction

During the preparation of the compounds $Cu(terpy)_2X_2 \cdot nH_2O$ with $Cu(terpy)_2^{2+}$ cations, in which $Cu^{2+}$ is bonded to six N atoms in a strongly distorted octahedral coordination,[1,2] we observed the formation of the complexes $Cu(terpy)X_2 \cdot nH_2O$ also. In these compounds the $Cu^{2+}$ ions are bonded to three N atoms and two additional ligands. While the symmetry of the $Cu(terpy)_2$ entities is determined by a strong first-order Jahn-teller effect, the stereochemistry of the five-coordinated complexes can be discussed on the basis of a second-order Jahn-Teller effect with respect to the alternative trigonal-bipyramidal (TBP) and square-pyramidal (SP) geometry.[3] Electrostatic calculations[4,5] show that the TBP geometry—with longer axial than equatorial bond lengths—is energetically slightly more stable than the SP geometry with a contracted apical bond distance, if electronic effects are absent. We are interested in the question of whether the presence of the $d^9$ cation $Cu^{2+}$ will influence these relative stabilities and will consider this problem on a more general basis elsewhere.[3] In the following we will report about the crystal structures of $Cu(terpy)Cl_2 \cdot nH_2O$ with $n = 1$ and $n = 0$ and give the results of spectroscopic measurements on a series of mostly newly prepared complexes, $Cu(terpy)X_2 \cdot nH_2O$ ($X = Cl^-, Br^-, I^- NO_2^-, NO_3^-, F^-$). An interesting aspect in this connection is the correlation of the EPR spectra and the coordination geometries. This matter is rather complicated, however, because exchange interactions between $Cu^{2+}$ polyhedra with different orientations in the unit cell may be present.

## Experimental Section

**Preparation of the Compounds $Cu(terpy)_mX_2 \cdot nH_2O$. X = $Cl^-$.** Concentrated solutions of $CuCl_2 \cdot 2H_2O$ in water and terpyridine in ethanol are united in the molar ratio 1:2. The green precipitate corresponds to $m = 2$ with varying water content ($n \simeq 2$-4).[1,2] The solid compounds decompose to the complex with $m = 1$ and terpyridine, if they are sharply dried over $P_2O_5$ or cautiously heated. The process is reversible, as we have found by means of X-ray analysis and ligand field (Figure 1) and EPR spectroscopy. If one dissolves $CuCl_2 \cdot 2H_2O$ and terpyridine (molar ratio 1:1) in boiling water (concentrated solution), green crystals of $Cu(terpy)Cl_2$ with $n = 0$ and $n = 1$ form side by side on cooling. The dark green crystals, which precipitate from the mother liquor if it is slowly evaporated in air at room temperature, have exclusively $n = 1$, however. The compound with $n = 0$ is not hygroscopic but stable even in moist air. It had been prepared and characterized by X-ray powder diagrams earlier.[6] Anal. Calcd for $m = 2$, $n = 4$: C, 53.5; H, 4.5; N, 12.5. Found: C, 53.4; H, 4.0; N, 12.4. Calcd for $m = 1$, $n = 1$: C, 46.6; H, 3.3; N, 10.8. Found: C, 46.7; H, 3.4; N, 10.9. Calcd for $m = 1$, $n = 0$: C, 49.0; H, 3.0; N, 11.4. Found: C, 48.8; H, 3.1; N, 11.2.

**X = $Br^-$, $I^-$.** The light green compound $Cu(terpy)Br_2$ is accessible indirectly by careful heating of $Cu(terpy)_2Br_2 \cdot 3H_2O$ or directly from hot solutions of $Cu(NO_3)_2$ and terpyridine by precipitation with a slight excess of KBr, by a procedure analogous to that described above. Brown crystals of $Cu(terpy)I_2$ are obtained by precipitation with KI. Anal. Calcd for X = $Br^-$: C, 39.5; H, 2.4; N, 9.2. Found: C, 39.8;

(1) W. Henke and D. Reinen, *Z. Anorg. Allg. Chem.*, **436**, 198 (1977).
(2) R. Allmann, W. Henke, and D. Reinen, *Inorg. Chem.*, **17**, 378 (1978).
(3) D. Reinen and C. Friebel, *Inorg. Chem.*, in press.
(4) R. J. Gillespie and R. S. Nyholm, *Q. Rev., Chem. Soc.*, **11**, 339 (1957).
(5) D. L. Kepert in "Inorganic Chemistry Concepts", Vol. 6, Springer-Verlag, New York, 1982, p 36.
(6) C. M. Harris, N. N. Lockyer, and N. C. Stephenson, *Aust. J. Chem.* **19**, 1741 (1966).

0020-1669/83/1322-2858$01.50/0 